Available online at www.sciencedirect.com
SCIENCE DIRECT
Catalysis Today 104 (2005) 86–93
CATALYSIS TODAY
www.elsevier.com/locate/cattod

Characteristics of Maya crude hydrodemetallization and hydrodesulfurization catalysts

Mohan S. Rana *, J. Ancheyta, S.K. Maity, P. Rayo

Instituto Mexicano del Petróleo, Eje Central Lázaro Cárdenas 152, México D.F., 07730 México City, Mexico

Available online 12 April 2005

Abstract

Hydrotreating of Maya crude is carried out under conditions close to the industrial operation. Various catalysts are prepared in the laboratory and the results are compared with a reference catalyst. Catalysts for such hydrotreating process are designed with high porosity and low active metal content considering metal deposition during the reaction and consequently the stability. Information regarding the activity and deactivation of the catalyst is discussed on the basis of catalyst porosity and deposited metal characterization. It was found that supports prepared by ammonium carbonate and urea hydrolysis methods have macro pore size distribution (PSD) as well as comparatively higher pore volume. The hydrodemetallization (HDM) activity increases while the hydrodesulfurization (HDS) activity decreases with increasing the average pore diameter (APD). The results of HDM and hydrodeasphaltenes (HDAs) activities of catalyst protrude distinct contribution of macro PSD of support which has more capabilities to retain metal deposition and better diffusion of complex organo-chelating metals. The spent catalysts are characterized by PSD, temperature-programmed reduction (TPR), in situ Fourier transform infrared (FT-IR), and transition electron microscopy (TEM). The spent and fresh catalysts characterization results are in well agreement with the activity. It has also been proposed that deposited vanadium sulfide may act as auto-catalytic activity for HDM and HDAs instead of being poison. It is also found that the deposition of metal depends on the porosity and surface area of the catalyst.

Keywords: HDS; HDM; HDAs; Catalyst deactivation; Metal deposition; FT-IR; TPR; Spent catalyst; Maya crude

1. Introduction

Upgrading the bottom of the barrel is one of the toughest challenges in heavy oil processing. The demand for heavy oil decreased recently due to their invaluable use as heavy feedstock while the need in light and middle distillate has moved to the opposite direction. The trend has indicated the importance of heavy oil processes which convert the heavy oil fraction into more valuable and environmental clean products. Therefore, now the important task in hydrotreating is heavy oils processing in which there is a lack of detailed knowledge about the feed composition. The composition and different molecular structure of crude oils consist predominantly of high concentration of heteroatoms hydrocarbons and vary with their origin [1,2]. Metals (V and Ni) are invariably the most abundant heteroatom impurities in heavy crudes. In general, metalloporphyrins are concentrated in the resin and mainly in the asphaltenes, which are building blocks of pyrrole. Nitrogen is present in the form of basic nitrogen compounds containing the pyridine nucleus, while the rest is mainly present in relatively non-basic compounds containing the pyrole nucleus [3]. Thus, the high-molecular-weight molecules are porphyrinic configurations of complex nickel and vanadyl radicals but these porphyrinic structures are not only metal carriers but also other hydrocarbons such as asphaltenes.

The hydrodemetallization (HDM) ends up in the metal sulfide accumulation onto the catalyst surface, and as a result, blocking of the active sites and pores [1,2,4]. This becomes more complicated since virtually infinite number of complex hydrocarbons like asphaltenes together with the molecules containing heteroatom, mainly S, N, V, Ni, etc., are present in high concentration [5]. In order to draw the concept governing the effect of support preparation in HDT catalysts performance, different γ-Al_2O_3 support preparation methods

* Corresponding author. Tel.: +52 55 9175 8418; fax: +52 55 9175 8429.
E-mail address: msingh@imp.mx (M.S. Rana).

0920-5861/$ – see front matter © 2005 Elsevier B.V. All rights reserved.
doi:10.1016/j.cattod.2005.03.059

have been employed to vary the porosity and PSD which play an important role in stability as well as in metal retention capacity on the surface of catalyst [1]. The different characterization of the catalysts before and after reaction provides important information about the role of textural properties on metal deposition. In general, the HDM catalysts behavior can be observed in two ways which depend on the textural properties of the catalyst, e.g. (a) micro-porous and low-range meso-porous catalyst decreases activity rapidly due to the pore mouth blockage and diffusion of complex molecules into the pores, (b) the catalysts containing macro-pores, in which deposited metal sulfides (V and Ni) behave themselves as catalytic sites, and those catalysts showed comparatively more stability during the time-on-stream (TOS). The metals from this hydrogenolysis are deposited on the catalyst in sulfided state, so that the reaction active sites were created with TOS; however, the original catalytic Mo sites may decrease due to the deposition of metal and asphaltenes [6].

Various researchers [7–14] focused on the effect of metallic deposits, mainly vanadium and nickel sulfides, which confirm that the decrease in activity is due to the metallic deposition on the catalyst surface. But only few characterization studies [15–18] have been carried out on spent catalysts. Toulhoat et al. [15,16] reported that nickel is always associated to vanadium and its crystallite size ranged from 5 to 30 nm, which grew up perpendicular to the alumina platelets. Kawada et al. [18] found that metals exist as the sulfide compounds using X-ray diffraction patterns. Smith and Wei [19–21] studied transition electron microscopy (TEM), EDX, STEM, and XPS for model molecules such as nickel etioporphyrin and vanadyl etioporphyrin on deactivated catalysts and concluded that nickel and vanadium sulfides deposited on HDM catalyst are in the form of relatively large spatially dispersed crystallites. Takeuchi et al. [6] reported X-ray power diffraction (XRD), ESR, and SEM on spent catalysts to find out the shape of deposited V and Ni sulfide crystallites. On the other hand, the surface deposited metal composition and its effect on the textural properties of spent catalyst at different catalyst beds is reported by Fleisch et al. [22].

In this publication we try to embark on an effect of support using different porosity and its influence on various catalytic activities such as HDM, hydrodeasphaltenes (HDAs), and hydrodesulfurization (HDS). The performance of the catalyst based on the pore size distribution (PSD) showed that larger the pore higher the HDM activity while the HDS activity decreases. The metal deposition capacity increases with high porosity which represents better stability of catalyst. The characterization results of fresh and spent catalysts showed that the number of catalytic sites altered after the reaction which is due to the deposited metal during the reaction. To show the chemical form of deposited species different analysis such as textural properties, TEM, FT-IR, and temperature-programmed reduction (TPR) characterization were carried out and the results indicated that the deposited species may have some catalytic activity.

2. Experimental

γ-Al_2O_3 supports were prepared by using different precipitation agents such as urea (γ-Al_2O_3-u), ammonium carbonate swing method (γ-Al_2O_3-acs), and ammonium hydroxide (γ-Al_2O_3-am). The details of the preparation of support are given elsewhere [23]. The Co–Mo promoted catalysts were prepared by the sequential incipient wetness impregnation method. The textural properties of these catalysts are given in Table 1.

The specific surface area (SSA), pore volume (PV), and PSD were carried out in a Quantochrome Nova 2000 equipment using N_2 adsorption–desorption at -196 °C. X-ray power diffraction patterns were collected on a Siemens D500 diffractometer using Cu Kα radiation. The TEM experiments were done in Jeol 100CX-II equipment.

TPR experiments were carried out in a flow apparatus, which consisted of a quartz reactor of 6 mm inner diameter designed by Altamira equipped with gas mass flow controllers. Feed gases were Ar (99.999% purity) and 10% H_2 (99.999% purity) balance in Ar. A thermal conductivity detector (TCD) was used to monitor the concentration of referred gases. Prior to each reduction experiment, the samples were pretreated at 450 °C (at the rate of 10 °C min^{-1}) with a flow of dry and purified Ar for 2 h. The experimental conditions for a TPR were a flow of 30 mL min^{-1}, with a 20 mg catalyst and a heating rate of 10 °C min^{-1}; final temperature was 1000 °C. The gas flow rate precisely controlled with an optional mass flow

Table 1
Textural properties of fresh and spent catalysts

Catalysts	Fresh catalysts			Spent catalysts		
	SSA (m^2/g)	PV (mL/g)	APD (nm)	SSA (m^2/g)	PV (mL/g)	APD (nm)
CoMo/γ-Al_2O_3-u	136	0.39	9.4	78	0.20	8.0
CoMo/γ-Al_2O_3-acs	160	0.47	11.2	80	0.25	7.2
CoMo/γ-Al_2O_3-UB	160	0.47	11.2	97	0.30	6.4
CoMo/γ-Al_2O_3-am	169	0.27	6.5	123	0.16	4.6
RC	175	0.56	12.7	140	0.21	6.0

SSA; PV; APD, average pore diameter; RC, reference catalyst for HDM feed, γ-Al_2O_3 + Ti 3.7 wt.%; U, spent catalyst (fixed bed 60 h TOS); BU, spent catalyst (batch reactor 6 h TOS).

controller accessory. The TCD records signals were taken as characteristic ''fingerprint'' of the sample.

Transition electron microscope (TEM) experiments were performed on sulfided spent catalysts after 60 h TOS, with a Jeol Model 100CX-II equipped with 100 kV acceleration voltages. After unloading, the catalysts were exposed to the air and washed with toluene and dried before the TEM analysis. Samples were grounded and catalyst particle were ultrasonically suspended in *n*-heptane and placed on a Cu grid coated with microgrid sputtered carbon polymer. At least 10 representative micrographs were taken for each catalyst surface investigated for MoS_2 and deposited metal entities.

The in situ FT-IR gas cell is configured with a liquid nitrogen MCT cryogenic detector. The spectra were recorded with a Nicolet 710 FT-IR spectrometer (4 cm^{-1} resolution, 128 scans and MCT cryo-detector) using a quartz vacuum cell with CaF_2 windows. The samples were used as a self-supported wafer (≈10–12 mg/cm^2) pressed at around 200 MPa. The catalysts were sulfided at 400 °C (1.5 °C min^{-1}) for 12 h with a mixture of H_2S (2 kPa) and H_2 (11 kPa).

The catalytic activities were carried out with a mixture of Maya crude and diesel 50/50 (w/w) in a high-pressure up-flow micro-reactor [23–25]. The diesel was used as diluent to avoid precipitation and gum formation during the feed processing. The properties of the feed are presented in Table 2. The metals (Ni, V), S, and N were analyzed in the feed and in the products by flame atomic adsorption spectrometry, UV-fluorescence, and chemiluminescence, respectively. Asphaltene is defined as the insoluble fraction in *n*-C_5. In a typical test, 10 mL (≈8.0 g) of catalyst was sulfided in situ with a mixture of DMDS and SRGO sulfiding feed (1 wt.% DMDS + SRGO) containing ≈2 wt.% 'S' and wet the catalyst bed at room temperature. The final conditions of sulfidation were 320 °C, 2.8 MPa for 5 h. After sulfidation, the flow was switched to the real feed (50 wt.% Maya and 50 wt.% diesel) and the following operating conditions were adjusted: temperature of 380 °C, LHSV of 1 h^{-1}, H_2/HC of 356 m^3/m^3 and pressure of 5.4 MPa [23].

One catalyst ($CoMo/Al_2O_3$-acs) was also tested against pure Maya crude feed using a Parr batch reactor. The properties of pure Maya crude are also given in Table 2. Before using in the batch reactor, a mass of oxidic catalyst (2.53 g) was dried at 150 °C for 1 h, then sulfided ex situ in a mixture of 12% H_2S in H_2 at 400 °C for 4 h in a fixed bed glass reactor operating at atmospheric pressure; the temperature was decreased to 25 °C, and finally the sulfided catalyst was flushed with inert gas for 5 h. The pure Maya crude (200 g) was poured into the autoclave and the sulfided catalyst was transferred into the reactor under inert atmosphere at room temperature. The reaction began when the agitation was started. The reaction was kept at 380 °C, under 10 MPa of H_2, with agitation speed of 750 rpm during 6 h. Then the catalyst and product mixture was separated and analyzed.

Table 2
Feed properties and its compositions

Properties	Maya crude	HDM (Maya crude + diesel) (50/50, w/w)
Elemental analysis (wt.%)		
C	86.9	84.2
H	5.3	8.8
N	0.3	0.184
S	3.52	2.21
Metal (wppm)		
Ni	49.5	26.21
V	273.0	124.78
Ni + V	322.5	150.99
Ca	11.26	5.0
Mg	2.04	1.01
Na	44.83	21.2
K	20.25	10.2
Fe	2.16	1.02
Asphaltene (wt.%) (*n*-C_5 insol.)	12.7	8.43
Physical properties		
Density (20/4 °C)	0.9251	0.88
Pour point (°C)	−30	−15
Ramscarbon (wt.%)	10.87	5.45
API gravity	21.31	37.09
Viscosity (g/(cm s)) at		
50 °C		3.08
100 °C		9.45

3. Results and discussion

3.1. Support preparation

The different γ-Al_2O_3 supports were prepared by aqueous solutions of aluminum nitrate urea, ammonium carbonate, and ammonia in which precipitant is obtained by in situ hydrolysis. The different parameters such as aging time, pH, precipitating agents, concentration of solution, etc. were considered to play an important role to generate the textural properties of the support. The prepared catalysts showed either macro-porous or higher range of meso-pores after active metal impregnation. The details regarding the preparation of support are reported elsewhere [23].

3.2. Textural properties

The pore volume and pore size distribution were carried out on fresh and spent catalysts and the results are reported in the Table 1. The pore size distribution of the fresh and the spent catalysts are presented in Fig. 1. This figure indicates that pores are moderately changed after 6 h and severely affected after 60 h TOS in the batch and micro-reactor reactors, respectively. We have also observed that both pore volume and specific surface area are reduced by 40–60% during the hydroprocessing reaction. The major loss in pore size distribution is observed in the micro-porous range; however, the losses in the range of meso- or macro-porous

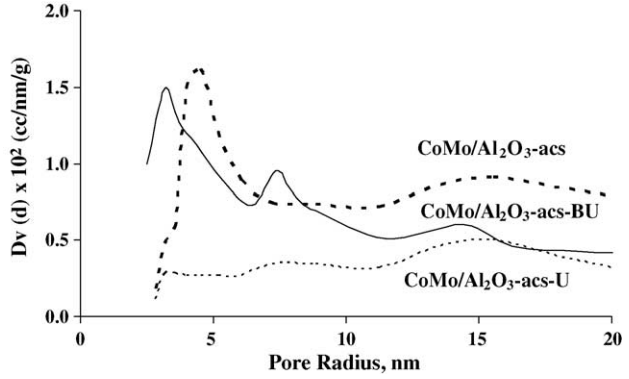

Fig. 1. A comparison of PSD of fresh and spent catalysts: CoMo/γ-Al_2O_3-acs-fresh; CoMo/γ-Al_2O_3-acs-UB (batch reactor spent catalyst); CoMo/γ-Al_2O_3-acs-U (fixed bed spent catalyst).

Table 3
N_2 adsorption–desorption measurements of pore mouth plugging

Catalysts	Area isotherm (absolute value)	*D*/*A*	*D*/BET	*A*/BET
CoMo/Al_2O_3-acs	0.0274	1.0	1.1	1.1
CoMo/Al_2O_3-acs-BU	–	1.3	1.2	0.9
CoMo/Al_2O_3-acs-U	0.0990	1.6	1.5	0.9
RC	–	1.1	1.0	1.0
RC-U	–	1.5	1.5	1.0
CoMo/Al_2O_3-am	0.0564	1.1	1.1	1.0
CoMo/Al_2O_3-am-U	0.4262	1.6	1.9	1.1

A, pore area calculated from BJH adsorption data; *D*, pore area calculated from desorption data; BET, total BET surface area; U, spent catalyst (fixed bed 60 h TOS); BU, spent catalyst (batch reactor 6 h TOS).

slightly vary. These results support the stable conversion for HDM and HDS after 60 h TOS [23].

In general, the stability of the crude oil processing catalyst is an important parameter and one of the major factors responsible for the nature of pore, metal sulfide, and coke deposition near the catalyst pore exterior surface which could prevent fully utilization of the interior pore volume. Thus, now is it more important to know how pore size distributions affect the pore plugging? In this regard, the relative nitrogen adsorption–desorption isotherms of fresh and spent catalysts are shown in Fig. 2a and b. These figures represent a large increase in the isotherm loops of the spent catalyst. The absolute areas are shown in Table 3 which were calculated using the trapezoidal rule integration method. The increase in isotherm loop and the reduction in total pore volume were considered as representative of deactivation via pore mouth coking. Two different catalysts were compared and severe deactivation on pore mouth plugging was showed with decreasing the total pore volume of the catalyst.

In Table 3, different surface areas and their relation to the pore plugging are presented. When the pores are cylindrical (fresh catalysts), the probable nitrogen desorption to adsorption area ratio must be close to unity, whereas the ratio increased up to 1.6 in case of spent catalyst. Indeed, "*ink-bottle*" types of pores are expected to be difficult to desorb until the relative pressure is quite low to allow nitrogen physisorbed from the narrow neck of pores. During this process, the interior volume of ink-bottle pore frees to desorb which results in large desorption–adsorption area ratio. It might be possible that adsorbed nitrogen in such type of pores exists as liquid which is comparatively difficult to desorb and, as a result, the evaporation process takes place progressibly rather than abruptly. It is pertinent to mention that the same effect has also been predicted theoretically for tubular structures of low-connectivity [26] samples. Therefore, the greater desorption–adsorption (BET-D/BET-A) area can be observed in the case of spent catalysts and this is more obvious in case of CoMo/Al_2O_3-am-U, in which the APD is 6.5 nm. The difference in adsorption–desorption surface area is another reason to confirm pore mouth plugging. These results further indicated that true pore size distribution should be calculated using adsorption data; however in the case of effective pore size distribution, desorption data are considered more reliable. Demetallation catalysts are largely distinguished by their pore size distribution (PSD) and average pore diameter (APD); greater than 10 nm pores are commonly used to increase

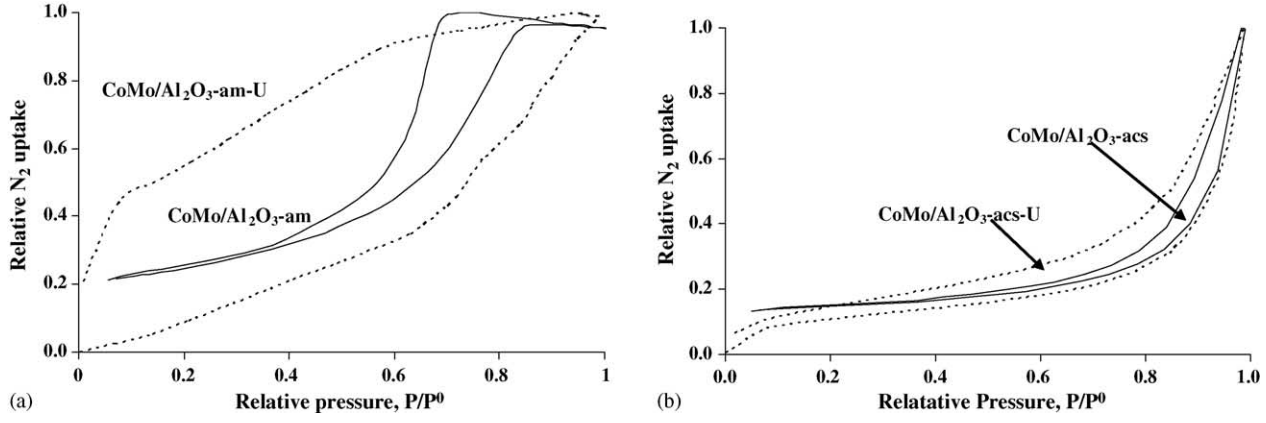

Fig. 2. Fresh and spent catalysts adsorption–desorption isotherms: (a) Al_2O_3-am; (b) Al_2O_3-acs.

diffusion of asphaltene into the interior of the catalyst and to provide more tolerance to the deposited metal sulfides. Tamm et al. [27] clearly demonstrated that demetallation is a diffusion-controlled reaction and the larger the pore diameter the higher the metal retention capacity with even distribution of metal (V and Ni) on cylindrical-shape catalyst. Green and Broderick [28] also found that large-pore catalysts have even more distribution of contaminant metal than the small-pore catalysts. Thus, the results of the hysteresis area moderately increase in the case of CoMo/Al_2O_3-acs-U compared with the CoMo/Al_2O_3-am-U, which indicate that large-pore catalyst has slower pore mouth plugging and tolerance for more metal.

3.3. Transition electron microscopy

TEM results of the spent catalysts further confirmed that V and Ni sulfides are deposited on the surface of catalysts in rod-shaped crystallites. It is also possible that nickel may associate with vanadium [Ni(V_3S_4)] which grew perpendicular on the surface of support. Similar kind of TEM results were obtained by Smith and Wei [19] for the HDM of model molecules. The MoS_2 slabs/stacks reduce drastically in spent catalysts due to the deposition of contaminants and metal (V, Ni) sulfide crystals [20]. However, greater number of acicular or rod-shaped crystallites were observed in the case of CoMo/Al_2O_3-acs-U and compared with CoMo/Al_2O_3-am-U catalyst as shown in Fig. 3a and b. These results indicate that CoMo/Al_2O_3-acs is having higher capacity to retain metals (Ni, V) due to the greater average pore diameter, i.e. 11.2 nm, while CoMo/Al_2O_3-am has 6.5 nm. It should be mentioned that the spent catalysts were exposed to air and washed with toluene before TEM analysis, which is an unavoidable process in the case of Maya crude spent catalyst which may cause some variation in oxidation state of V and Ni sulfides [22]. Similar results [23] were observed in XRD pattern of spent catalyst (after 60 h TOS) which were carried out in order to see the metal deposition (Ni and V) on the outer surface of catalyst. Deposited metals exist as the sulfide compounds and are attributed to the V_3S_4, V_2S_3, and Ni_3S_2 phases [6].

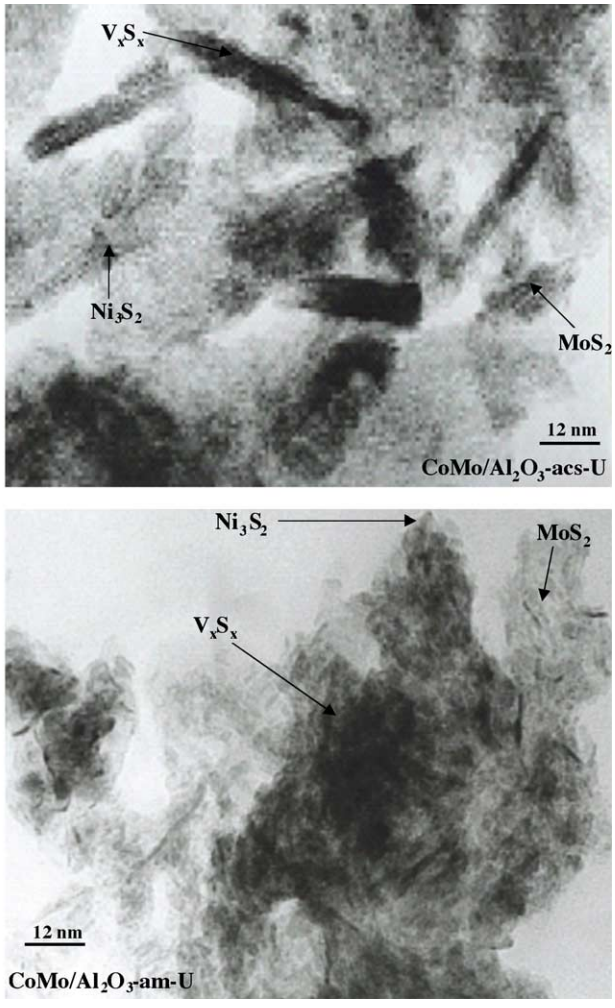

Fig. 3. TEM analyses of the spent catalysts: (a) CoMo/γ-Al_2O_3-acs-U; (b) CoMo/γ-Al_2O_3-am-U.

3.4. Surface composition of active metal sites

Nickel and vanadium sulfides are deposited on the surface of catalyst which is responsible for pore plugging, but on the other side, these deposited sulfides may be acting as "*active sites*" or auto-catalysis. Therefore, a qualitative measure of active site would be required, but unfortunately it becomes extremely complicated to find out the concrete information about the deposited metal sulfides and active sites. Two experiments were performed using low-temperature CO chemisorption to find out a rough measurement of active site density as shown in Fig. 4. We cannot exclude the formation of particular site existed by the Ni and V sulfides. The fresh catalyst showed supported (MoS_2) and promoted sites (Co–Mo–S) at around 2155 and 2112 cm^{-1}, respectively. These bands attributed to the CO interaction with the MoS_2 and its edges [29,30]. However, in the case of spent catalyst higher CO chemisorption indicated that the deposited metal sulfides are somehow responsible for producing some catalytic sites at the expense of pore mouth plugging and may be diminishing the supported and promoted original active sites (Mo-CUS). In this respect deeper studies will be necessary to quantify active sites and distinguish between original (Mo, CoMo) and deposited metals (Ni and V) sulfide sites.

3.5. Temperature-programmed reduction of (TPR) fresh and spent catalysts

The interaction between Mo and the support was studied by TPR. To distinguish the interaction of deposited metals (Ni, V) species, spent catalysts were also measured as shown in Fig. 5a and b. The TPR pretreatment and experimental conditions were similar for fresh and spent catalysts. For

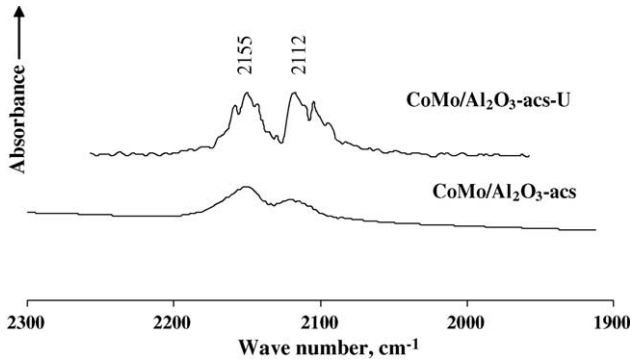

Fig. 4. Infrared spectra of CO chemisorption on the sulfided fresh and spent catalysts.

$CoMo/Al_2O_3$-acs (Fig. 5a) two main peaks were found, the first at 482 °C and the second at 878 °C. The low-temperature peak can be assigned to partial reduction Mo^{6+} to Mo^{4+}, multilayer molybdenum oxide or octahedral molybdenum species [31,32]. The high-temperature peak at 878 °C is considered to be related to deeper reduction of molybdenum oxide along with tetrahedral species. We did not find any indication for Co reduction peak but Co may facilitate the Mo reduction peaks at lower temperature. On the other hand, the spent catalyst showed two distinct peaks at 275 and 508 °C and a broad shoulder was observed at temperature greater than 1000 °C; unfortunately, due to limitation of the instrument, this peak could not be clearly observed. The low-temperature peak at 275 °C may be due to the deposited nickel species. To find out the better insight of these TPR results the fresh reference catalyst (RC) as well as its spent catalyst TPR finger prints were carried out and are shown in Fig. 5b along with pure V_2O_5. For the fresh reference catalyst (RC) $NiMo/Al_2O_3$–TiO_2 (TiO_2 = 3.7 wt.%), the TPR peaks were found at 418 °C, and shoulders at 502 and 819 °C. The peaks at 418 and 819 °C are due to the different species of Mo as indicated above; the different location of these peaks may be due to the different interaction of active metal with the support, while the peak at 502 °C is assigned to the intermediate species formation due to the NiMo. The spent catalyst profile is more likely assigned to the alumina-supported spent catalyst (Fig. 5a); however, pure V_2O_5 oxide showed two typical peaks, in which the high temperature peak at around 1000 °C well match with the spent catalyst peak. Thus, it is clear that nickel and vanadium sulfides are strongly interacting with the support surface; in other words, these species are similar to Mo and Co.

4. Catalytic activities

In Fig. 6, a comparison has been made for different catalysts activities after 60 h time-on-stream including reference one which contains higher amount of Mo as well as 3.5 wt.% of TiO_2. The HDM activity among all lab-prepared catalysts containing Co–Mo is slightly better for $CoMo/\gamma$-Al_2O_3-acs while the smallest pore catalyst ($CoMo/\gamma$-Al_2O_3-am) showed lower activity for HDM. Thus, the PSD is in good agreement with HDM conversion. The low conversion in the case of $CoMo/\gamma$-Al_2O_3-am is due to its pore distribution in the range of 5–15 nm while the other catalysts have macro pore size profile in the range of 20–200 nm. As an effect of average pore diameter the different activities are shown in Fig. 7. The comparison between HDM and HDS showed opposite trends which revealed that HDM catalyst should be essentially macro-porous in nature. Thus, HDM conversion is limited in the case of $CoMo/\gamma$-Al_2O_3-am due to the penetration of porphyrins or metal-chelating compounds into the pores. The Maya crude contains significant amount of asphaltene which are responsible for catalyst deactivation in hydroprocessing along with metal deposition. It is observed that HDM as well as HDAs significantly depend on the catalyst pore structure while the HDS activity may depend on the dispersion of the active metal [33]. These results indicated that the HDS activity distinctively differ from the HDM and HDAs. Most probably the HDS activity appreciably depends on the surface area and the active sites. $CoMo/Al_2O_3$-am showed the lowest activity for HDM and HDAs while maximum

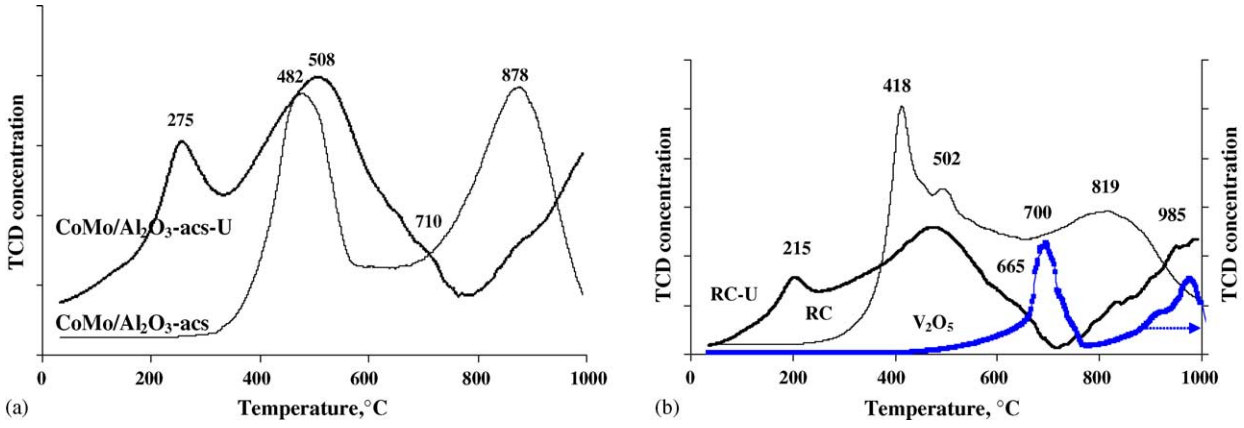

Fig. 5. Fresh and spent catalysts TPR patterns: (a) $CoMo/Al_2O_3$-acs; (b) reference catalyst and comparison with V_2O_5.

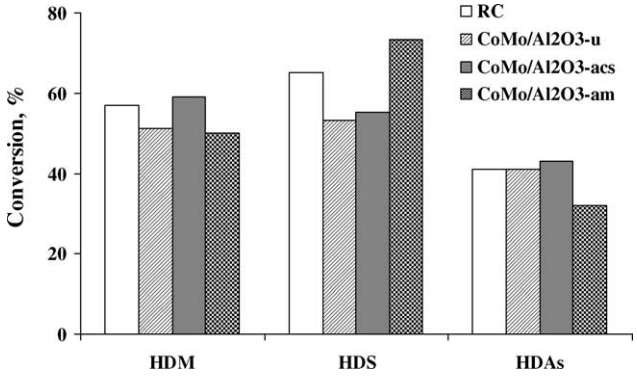

Fig. 6. Catalytic activity with different catalysts after 60 h TOS.

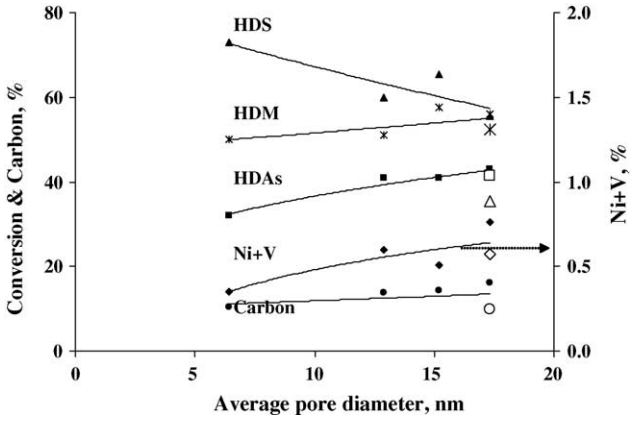

Fig. 7. Effect of average pore diameter on conversion and deposition of carbon and metal: solid symbol, fixed bed reactor (60 h TOS); open circle, batch reactor (6 h TOS).

activity can be seen for HDS (Fig. 6). Thus, HDM and HDAs conversions are limited due to the diffusional limitations of complex metalloid and asphaltenes molecules for the catalyst having less than 10 nm pore diameter. Thus, the performance of heavy oil HDT process with regard to different functionalities, such as HDM, HDS, and HDAs, is clearly linked to the porosity and nature of the heavy crude oil. The expected reasons of decreasing HDS activity is the blocking of active sites and the deposition of carboneous and metallic impurities in the interstices between the catalyst particles. The quantification of diffusivity could be calculated using the approach taken by Wiesz and Schwartz [34] which provides a basis for interpreting the apparently diffusivities using specific surface area, pore volume, and particle density.

Different catalyst results show that the metallic deposition on the catalyst surface is more of the V metal sulfides that deposited as larger crystallite than Ni as shown by the TEM micrographs. The XRD and TEM results indicate that Ni is subtlety distributed on the catalyst surface in comparison with V. The TEM and XRD results also showed higher deposition of metal on bigger pores with rod-shaped crystalline phases while low-porosity catalysts are randomly oriented with overlapping irregular shape of crystallites. Other characterization results of spent catalyst showed that the higher the APD the greater the carbon deposition and S/Mo ratio, and hence the greater the stability or metal retention capacity of catalyst. It is also strongly expected that the deposited V_xS_x phases provide some activity on the surface of the catalyst. Thus, HDM catalyst should be essentially macro-porous in nature while HDS conversion is hardly affected by porosity.

The $CoMo/Al_2O_3$-acs catalyst was also tested against the pure Maya crude in a batch reactor and the activities were observed after 6 h as shown in Fig. 8a. It has to be pointed out that with pure Maya crude the HDM as well as HDS activities were lower than fixed bed flow reactor (diluted feed) but higher selectivity can be observed in Fig. 8b after 6 h TOS for both feedstocks. The HDM selectivity reduces with TOS which indicates that on decreasing the mouth of the pores the HDS activity increases while HDM activity decreases. Thus, the nickel and vanadium sulfides may inhibit HDS reactions, whereas they do have some HDM activity.

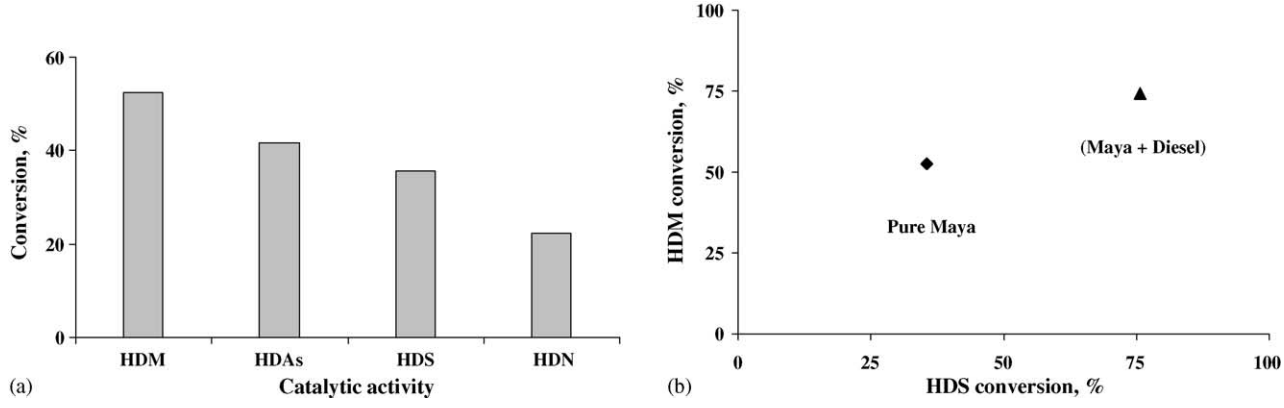

Fig. 8. (a) Catalytic activities for Maya crude in batch reactor. (b) HDM selectivity as an effect of feed composition.

5. Conclusion

The wide range of spent catalyst characterization indicates that the catalysts pores are plugged during the heavy oil processing. The V and Ni presence are consistent and identified as V_3S_4 and N_3S_2 by TEM, XRD, and TPR. The coke deposition preferentially took place at the entrance of pores leading to 30–70% decrease in the specific surface area and total pore volumes and an increase in area of adsorption–desorption isotherm which represent nature and behavior of pore in spent catalysts. The qualitative analysis of surface metal composition as well as TPR results indicated that deposited metal (V, Ni, etc.) modify the surface and may change the nature of original active site presented by Mo and CoMo.

The effect of support preparation on the pore size distribution and average pore diameter apparently controls the catalytic activities of heavy crude oil. HDM and HDAs activities significantly depend on the catalyst pore size distribution while the HDS activity may depend on the metal dispersion and surface area of supported catalysts. The hydrogenolysis reaction is accompanied by the accumulation of the deposited metals within the catalyst or autocatalysis. The effect of textural properties of the catalyst on the metal retention capacity and stability is clearly demonstrated, that is, large-pore catalyst showed slower pore mouth plugging and a tolerance for more metal.

Acknowledgements

M.S.R thanks to I.M.P. for providing PDF. We express our appreciation to Mr. Jose G. Espinosa and Mrs. Bertha Nuñez for helping in preparation of feeds and adsorption–desorption experiments.

References

[1] J.G. Speight, The Chemistry and Technology of Petroleum, Marcel Dekker, New York, 1992.
[2] H. Topsøe, B.S. Clausen, F.E. Massoth, in: J.R. Anderson, M. Boudart (Eds.), Hydrotreating Catalysis—Science and Technology, vol. 11, Springer-Verlag, New York, 1996.
[3] J.F. Le Page, J. Cosyns, P. Courty, E. Freund, J.-P. Franck, Y. Jscquin, B. Juguin, C. Marcilly, G. Martino, J. Miquel, R. Miquel, R. Montarnal, A. Sugier, H. Van Landeghem, Applied Heterogeneous Catalysis, Design, Manufacture, Use of Solid Catalysts, Technip, Paris, 1987.
[4] E. Furimsky, F.E. Massoth, Catal. Today 52 (1999) 381.
[5] J.W. Gosselink, CatTech 2 (1998) 127.
[6] C. Takeuchi, S. Asaoka, S.-i. Nakata, Y. Shiroto, Am. Chem. Soc. Prepr. Div. Petrol. Chem. 30 (1) (1985) 96.
[7] M. Marafi, A. Stanislaus, Appl. Catal. A 159 (1997) 259.
[8] H. Koyama, E. Nagai, H. Kumagai, ACS Symp. Ser. 634 (1996) 208.
[9] B.J. Johnson, F.E. Massoth, J. Bartholdy, AIChE J. 32 (1986) 1980.
[10] G. Gualda, S. Kasztelan, Stud. Surf. Sci. Catal. 88 (1994) 145.
[11] G. Gualda, S. Kasztelan, J. Catal. 161 (1996) 319.
[12] J. Bartholdy, B.H. Cooper, in: M. Absi-Halabi, et al. (Eds.), Catalyst in Petroleum Refining and Petrochemical Industries, Elsevier, Amsterdam, 1995, p. 117.
[13] F.X. Long, B.S. Gevert, P. Abrahamsson, J. Catal. 222 (2004) 6.
[14] R.L.C. Bonné, P. Van Steenderen, A.E. Van Diepen, J.A. Moulijin, Appl. Catal. A 108 (1994) 171.
[15] H. Toulhoat, R. Szymanski, J.C. Plumail, Catal. Today 7 (1990) 531.
[16] H. Toulhoat, J.C. Plumail, C. Houpert, R. Szymanski, P. Bourseau, G. Muratet, Advances in residue upgrading, Am. Chem. Soc., Div. Petrol. Chem. 32 (2) (1987) 463.
[17] S. Eijsbouts, Stud. Surf. Sci. Catal. 127 (1999) 21.
[18] I. Kawada, M.N. Onoda, M. Ishii, M. Nakahira, J. Solid State Chem. 15 (1975) 246.
[19] B.J. Smith, J. Wei, J. Catal. 132 (1991) 1.
[20] B.J. Smith, J. Wei, J. Catal. 132 (1991) 41.
[21] B.J. Smith, J. Wei, J. Catal. 132 (1991) 21.
[22] T.H. Fleisch, B.L. Meyers, J.B. Hall, G.L. Ott, J. Catal. 86 (1984) 147.
[23] M.S. Rana, J. Ancheyta, P. Rayo, S.K. Maity, Catal. Today 98 (2004) 151.
[24] L.C. Castañeda, F. Alonso, J. Ancheyta, Stud. Surf. Sci. Catal. 133 (2001) 477.
[25] S.K. Maity, J. Ancheyta, L. Soberanis, F. Alonso, M.E. Llanos, Appl. Catal. A 244 (2003) 141.
[26] F. Rojas, I. Kornhauser, C. Felipe, J.M. Esparza, S. Cordero, A. Domínguez, J.L. Ricardo, Phys. Chem. Phys. 4 (2002) 2346.
[27] P.W. Tamm, H.F. Harnsberger, A.G. Bridge, IEC Proc. Des. Dev. 20 (1981).
[28] D.C. Green, D.H. Broderick, Chem. Eng. Prog. 77 (12) (1981) 33.
[29] A. Travert, C. Dujardin, F. Maugé, S. Cristol, J.F. Paul, E. Payen, D. Bougeard, Catal. Today 70 (2001) 255.
[30] A. Travert, Ph.D. thesis, University of Caen, France, 2000.
[31] M. Henker, K.P. Wendlandt, J. Valyon, P. Bormmann, Appl. Catal. A 69 (1991) 205.
[32] P. Arnoldy, J.C.M. de Jorge, J.A. Mouljin, J. Phys. Chem. 89 (1985) 4517.
[33] S. Eijsbouts, J.J.L. Heinemann, H.J.W. Elzerman, Appl. Catal. A 105 (1993) 69.
[34] P.B. Weisz, A.B. Schwartz, J. Catal. 1 (1962) 399.